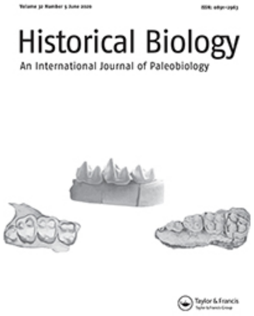

Taylor & Francis
Taylor & Francis Group

Historical Biology

An International Journal of Paleobiology

ISSN: (Print) (Online) Journal homepage: https://www.tandfonline.com/loi/ghbi20

Evolutionary disparity in the endoneurocranial configuration between small and gigantic tyrannosauroids

Martin Kundrát , Xing Xu , Martina Hančová , Andrej Gajdoš , Yu Guo & Defeng Chen

To cite this article: Martin Kundrát , Xing Xu , Martina Hančová , Andrej Gajdoš , Yu Guo & Defeng Chen (2020) Evolutionary disparity in the endoneurocranial configuration between small and gigantic tyrannosauroids, Historical Biology, 32:5, 620-634, DOI: 10.1080/08912963.2018.1518442

To link to this article: https://doi.org/10.1080/08912963.2018.1518442

Published online: 19 Sep 2018.

HISTORICAL BIOLOGY
2020, VOL. 32, NO. 5, 620–634
https://doi.org/10.1080/08912963.2018.1518442

ARTICLE

Evolutionary disparity in the endoneurocranial configuration between small and gigantic tyrannosauroids

Martin Kundrát[a], Xing Xu[b], Martina Hančová[c], Andrej Gajdoš[c], Yu Guo[d] and Defeng Chen[e]

[a]Centre for Interdisciplinary Biosciences, Technology and Innovation Park, Pavol Jozef Šafárik University, Košice, Slovak Republic; [b]Key Laboratory of Vertebrate Evolution and Human Origin of Chinese Academy of Sciences, Institute of Vertebrate Paleontology and Paleoanthropology, Chinese Academy of Sciences, Beijing, China; [c]Institute of Mathematics, Faculty of Science, Pavol Jozef Šafárik University, Košice, Slovak Republic; [d]The Geological Museum of China, Beijing, China; [e]Beijing Higher Institution Engineering Research Center of Computerized Tomography, Capital Normal University, Beijing, China

ABSTRACT

In extinct archosaurs, brain proportions have been inferred from the morphology of fossilized endocasts. Here we provide the first neurocranial and paleoneurological description of the basal, small-bodied tyrannosauroid *Dilong paradoxus* compared with larger tyrannosaurids, like *Tyrannosaurus rex*. *Dilong* differs from other tyrannosauroids in the proportions of cerebral and cerebellar regions, morphology of venous sinuses, and superimposed position of the forebrain relative to the rest of the endocast. Whereas endocasts of *Tyrannosaurus* show a more linear configuration and likely contained within a thick interstitial space, the endocast of *Dilong* indicates an S-shaped brain protected by thinner meninges. Based on our statistic analysis and comparisons with modern crocodilians, we hypothesize that increased body size likely imposed a new spatial configuration for development of the central nervous system during the evolution of gigantism in tyrannosaurs.

ARTICLE HISTORY
Received 12 July 2018
Accepted 29 August 2018

KEYWORDS
Dinosauria; tyrannosauroidea; endocast; brain; evolution

Introduction

The central nervous system (CNS) controls cognitive and sensory-motor mechanisms of behavioral interactions, and therefore has played a major role in the evolutionary adaptation of vertebrates (Butler and Hodos 2005). Direct relations between the CNS and behavior are difficult to infer for extant animals, and thus much more so for those that lived millions years ago. Structural studies of the CNS are further limited if not impossible because the brain itself is composed of soft tissue and rarely, if ever, fossilizes (Rogers 1998). More likely, but extremely rare, are fossils or even a series of fossils from the same species or close relatives that record both behavioral indicators and paleoneurological traits (Rich and Rich 1988). Despite these constraints, the number of studies in paleoneurology has substantially increased over last two decades. This is mostly due to the advancements in X-ray imaging technology (Witmer et al. 2008), discovery and availability of new specimens (Domínguez Alonso et al. 2004; Knoll and Schwarz-Wings 2009; Balanoff et al. 2013; Lauters et al. 2013), and comparative neontological studies (Dooling et al. 2000; Hullar 2006; Corfield et al. 2008; Iwaniuk et al. 2009; Sol et al. 2010) that provide an experimental base for better-constrained interpretations in paleoneurology. In comparison with previous studies (Hopson 1979), noticeable progress has recently been made in our understanding of the details in endoneurocranial evolution within some of dinosaurs groups. Several recent studies have provided valuable paleoneurological descriptions of particular groups (e.g. ceratopsians (Witmer and Ridgely 2008), sauropods (Sereno et al. 2007; Balanoff et al. 2010; Knoll et al. 2012; Paulina-Carabajal 2012), ceratosaurs (Sanders and Smith 2005; Sampson and Witmer 2007; Paulina-Carabajal and Succar 2015; basal tetanurans (Larsson 2001; Franzosa and Rowe 2005; Paulina-Carabajal and Canale 2010; Paulina-Carabajal and Currie 2012), coelurosaurs (Osmólska 2004; Kundrát 2007; Balanoff et al. 2009; Witmer and Ridgely 2009; Alifanov and Saveliev 2011; Lautenschlager et al. 2012)), neuro-morphological variability inside well-known groups (e.g. hadrosaurids (Evans et al. 2009), tyrannosaurids (Witmer and Ridgely 2009)), ontogentic variability (e.g. psittacosaurs (Zhou et al. 2007), dryosaurids (Lautenschlager and Hübner 2013)), and adaptional trends (Larsson et al. 2000; Zelenitsky et al. 2011).

The endoneurocranial anatomy of tyrannosaurs has been the most intensively studied among coelurosaurian theropods. The original description of *Tyrannosaurus* (Osborn 1912) refined by later studies (Hopson 1979; Brochu 2000, 2003; Witmer and Ridgely 2009; Hurlburt et al. 2013), has subsequently been compared to taxa such as '*Nanotyrannus*' (Witmer and Ridgely 2009), *Tarbosaurus* (Saveliev and Alifanov 2007), *Gorgosaurus* (Witmer and Ridgely 2009) and *Alioramus* (Brusatte et al. 2009; Bever et al. 2011, 2013). Tyrannosaurs probably originated by the Middle Jurassic (Rauhut et al. 2010), and their evolution is characterized by extreme size change leading to the origin of hypercarnivorous giants (Holtz 2004). Tyrannosaurid gigantism has been proposed to have evolved primarily through the acceleration of growth rates (Erickson et al. 2004) (peramorphosis), resulting in multi-ton predators far exceeding the size of basal

CONTACT Martin Kundrát martin.kundrat@upjs.sk Centre for Interdisciplinary Biosciences, Technology and Innovation Park, Pavol Jozef Šafárik University, Košice 04154, Slovak Republic

Published online 19 Sep 2018

tyrannosauroids (e.g. *Kileskus* (Averianov et al. 2010), *Proceratorsaurus* (Rauhut et al. 2010), *Guanlong* (Xu et al. 2006), *Dilong* (Xu et al. 2004), *Stokesosaurus* (Mades 1974)) by approximately 90-to-100 fold.

Although the skeletal hallmarks of tyrannosauroid adaptations towards gigantism are well known (Holtz 2004; Sereno et al. 2009), the response of the CNS is still undocumented. Such an understanding requires two levels of data differences spanning juvenile through adult phenotypes of the same species and inter-specific morphological variation in the smallest to the largest taxa. Insight into the endoneurocranial ontogeny of tyrannosaurids might be accomplished if one accepts that *Nanotyrannus* (Bakker et al. 1988) represents a skeletally immature *Tyrannosaurus* (Carr 1999) althought this issue remains controversial even after thoroughful CT-based analysis of the cranium (Witmer and Ridgely 2010). Similar controversy concerning ontogentic maturity surrounds the small-bodied tyrannosaurid *Raptorex* (Sereno et al. 2009; Fowler et al. 2011). Finally, although not controversial, but still awaiting the comparative study, is the endoneurocranium of the juvenile *Tarbosaurus* (Tsuihiji et al. 2011). Recent progress has been made in accessing morphological variation between tyrannosaurid taxa of considerably different body sizes. For example, there are significant differences in the 5-to-6 m long *Alioramus* (Brusatte et al. 2009, 2012; Bever et al. 2011, 2013) and *Tyrannosaurus* (Holtz 2004; Witmer and Ridgely 2009), which is approximately twice as long. Thus, what remains unknown is how tyrannosauroid endoneurocrania were configured prior to the evolution of gigantism.

The current paleobiological knowledge (Brusatte et al. 2010) and growing number of suitable fossils (e.g. ? juvenile *Raptorex* (Sereno et al. 2009), juvenile *Tarbosaurus* (Fowler et al. 2011), *Tarbosaurus* (Hurum and Sabath 2003), *Gorgosaurus* (Currie 2003), *Albertosaurus* (Currie 2003), *Daspletosaurus* (Currie 2003), *Teratophoneus* (Loewen et al. 2013), *Qianzhousaurus* (Lü et al. 2014)) makes tyrannosauroids the best model to investigate how the central nervous systems evolved during the transition from a small to becoming the very large terrestrial predators (Holtz 2004; Brussate et al. 2010a). Herein, we provide the first report about the configuration of the endoneurocraium in a small bodied tyrannosauroid *Dilong paradoxus* (Xu et al. 2004) (Figure 1(a)) that lived about 125 million years ago, some 50 million year before *T. rex*. Current cladistics analyses (Brusatte et al. 2009; Sereno et al. 2009; Brusatte et al. 2010; Rauhut et al. 2010; Tsuihiji et al. 2011; Loewen et al. 2013) imply that *Dilong* is a basally-diverging representative of non-proceratosaurid tyrannosauroids and as such could reveal the primitive conditions for Tyrannosauroidea. Following this phylogenetic placement we demonstrate that the endoneurocranium was considerably modified during the evolution of tyrannosauroids, and propose that the considerable differences in the endocast shapes between *Dilong* and *Tyrannosaurus* might be coupled with and primarily due to body enlargement.

Material

The specimen analyzed here is the skull of the holotype of *Dilong paradoxus* (IVPP [Institute of Vertebrate Paleontology and Paleoanthropology, Chinese Academy of Sciences, Beijing, China] 14243) which has been described as an individual approaching maturity (a sub-adult stage; Xu et al. 2004). This fossil was unearthed from beds of the Yixian Formation (western Liaoning) that are about 125 million years old (Pan et al. 2013).

Methods

CT data acquisition

CT scanning was performed at the Capital Normal University using a high energy cone-beam CT instrument. The X-ray image of the fossil was acquired at 350 kV and 2.5 mA, with the focus-to-detector distance (FDD) of 1360 mm, focus-to-object distance (FOD) of 1175 mm. FDK (Feldkamp, David and Kress) reconstruction algorithm was used to produce 3D array of attenuation measurements with dimensions of 1024 × 1024 x 1600, corresponding spatial resolution was 0.15 mm. The large array was resampled to 512 × 512 x 800 to reduce the overall size of the data set in order to facilitate processing.

3D Imaging

The CT scan of the IVPP 14,243 specimen of *Dilong* was processed by and volume rendering done with the software VGStudio MAX 3.0. Volumes were calculated using the voxel counting tool of VGStudio MAX 3.0. We refer to structures of the endocast of *Dilong* and *Tyrannosaurus* as if they were encephalic structures themselves.

Data analysis

The endocast shape of *Dilong* and 14 other theropod (*Alioramus* – Bever et al. 2011; *Allosaurus, Deinonychus, Gorgosaurus, Nanotyrannus, Tarbosaurus, Tyrannosaurus* 5029, 5117, 2081 – Witmer and Ridgely 2009; *Archaeopteryx* – Domínguez Alonso et al. 2004; *Carcharodontosaurus* – Larsson 2001; *Conchoraptor* – Kundrát 2007; *Giganotosaurus* – Paulina-Carabajal and Canale 2010; *Majungasaurus* – Sampson and Witmer 2007) taxa were first defined using tools in ImageJ in 2D, to be available for the geometric morphometric study. Subsequently, they were digitized using the R package geomorph (Adams et al. 2018; R Core Team 2018). In the first place, it was tested whether the digitization of landmarks itself did not cause a significant error. As a test statistic the difference in average Procrustes distances between the group of all the observed shapes and the copies of one individual (Webster and Sheets 2010) was applied. Since only 15 endocasts were considered, nonparametric bootstrap procedure was implemented by us. Nearest-neighbor analyses by testing the over-dispersion and clustering (Foote 1990; Zelditch et al. 2012) was used to validate the studied shapes. As the last initial verification, the tangent-space adequacy test was performed in TPSSmall (Rohlf 2010). Procrustes analysis itself and consequently the Principal component analysis (PCA) based on acquired Procrustes coordinates were both conducted with R package geomorph (Dryden and Mardia 2016; Adams et al. 2018). Regression analysis of body length dependence on PCA components as well as other graphical analyzes were performed in R software with multiple packages such as shapes and ape (Paradis et al. 2004; Dryden 2017; R Core Team 2018).

Results

Braincase preservation of dilong

Most of the braincase of *Dilong* (IVPP 14243) is encased in matrix and with none of the endoneurocranial cavity is exposed (Figure 1(b,c)). Therefore, the skull of IVPP 14243 was scanned using a cone-beam CT scanner in order to reconstruct a digital endocast. Parasagittal slices through the braincase (Figure 1(d,f)) reveal noticeably large proportions of some endoneurocranial regions, such as the cerebrum, mesencephalon and flocculus. Coronal slices also reveal that the endoneurocranial cavity has been considerably altered by multi-directional movements of the neurocranial bones (Figure 1(g,h)). In order to assess proportions of the endocast

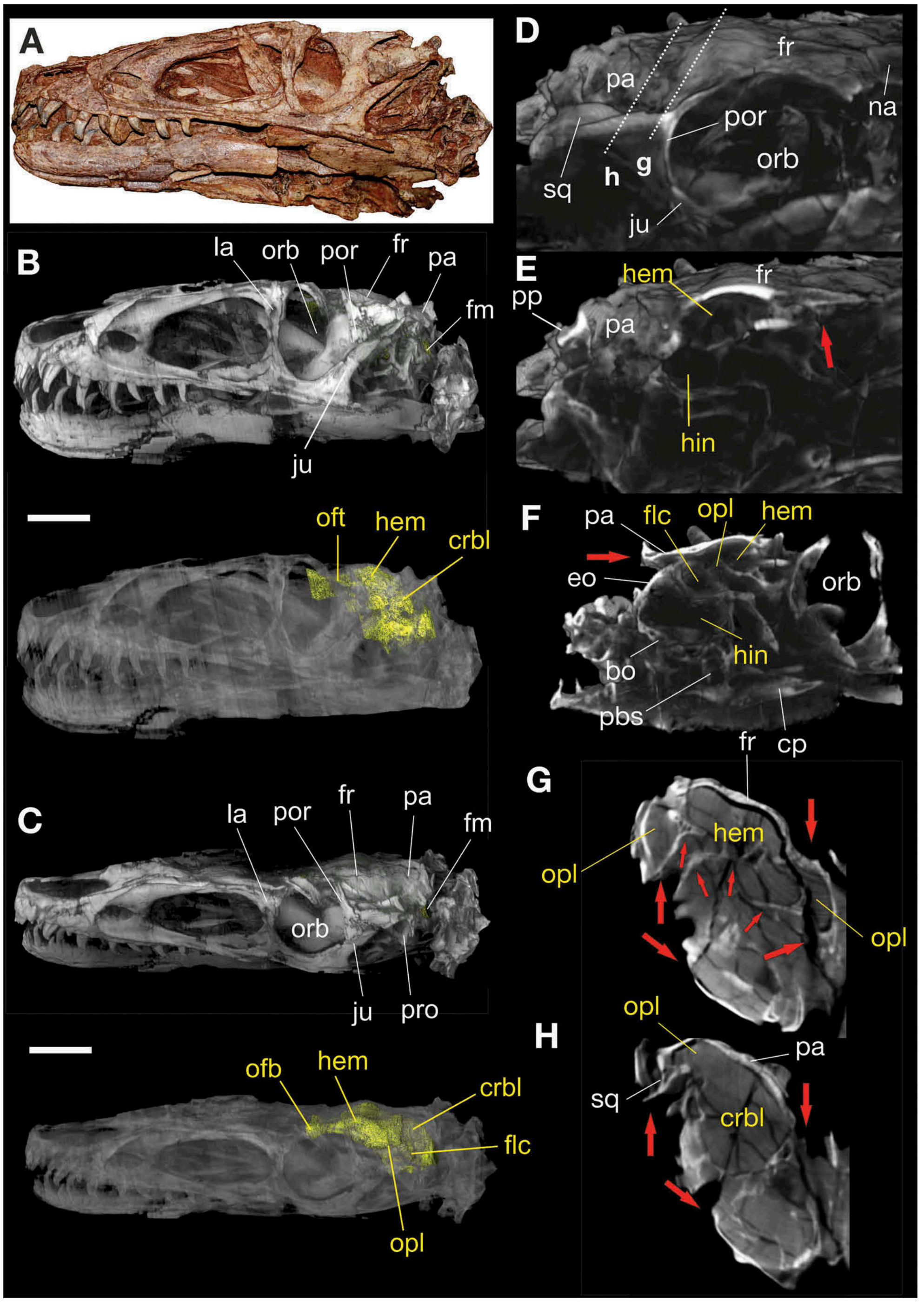

Figure 1. Skull of the basal tyrannosauroid *Dilong paradoxus* from the Lower Cretaceous of China. A, The skull of the holotype of *Dilong paradoxus* (IVPP 14,243) in left lateral view. **B**, Opaque and transparent renderings of the skull including the endoneurocranium (yellow) shown in lateral view. **C**, left lateral-dorsal view. **D-F**, Consecutive parasagittal CT projections (right lateral-to-medial) showing the endoneurocranial cavity of *Dilong*. **G, H**, Coronal CT projections showing deformation of the endoneurocranium of *Dilong*; Major directional shifts are indicated by large red arrows and intracranial bone dislocations are marked by small red arrows. Abbreviations: bo, basioccipital; eo, exoccipital; cp, cultriform process; crb, cerebellum cavity; crbl, cerebellum; flc, flocculus recess/flocculus; fm, foramen magnum; fr, frontal; hem, cerebral hemispheres sector; ju, jugal; la, lacrimal; mtc, metencephalic sector; na, nasal; ocd, occipital condyle; ofb, olfactory bulb; oft, olfactory tracts; opl, optic lobe reces/optic lobe; orb, orbit; pa, parietal; pbs, parabasisphenoid; por, postorbital; pp, paroccipital process; pro, prootic; sq, squamosal. Scale 15 mm (A-C).

of *Dilong* we checked endoneurocranial morphology in multiple cross-sectional perspectives (Figure 2).

Endocast of dilong paradoxus

We reconstructed the majority of the endocast of *Dilong* based on preserved endoneurocranial structures (Figure 3). The total volume and surface of the reconstructed endocast are 8.4 cm^3 and 30.8 cm^2, respectively. The olfactory tracts, roofed by the frontals, are lateromedially thick but thinner dorsoventrally. The olfactory tracts appear to be relatively short with the bulbs being as long as the tracts. Because we could not track the olfactory bulbs further anteriorly, we can only estimate their proportions from a distance between the position of the olfactory chamber of the nasal cavity and the mid-orbit level where the olfactory tracts are about to expand.

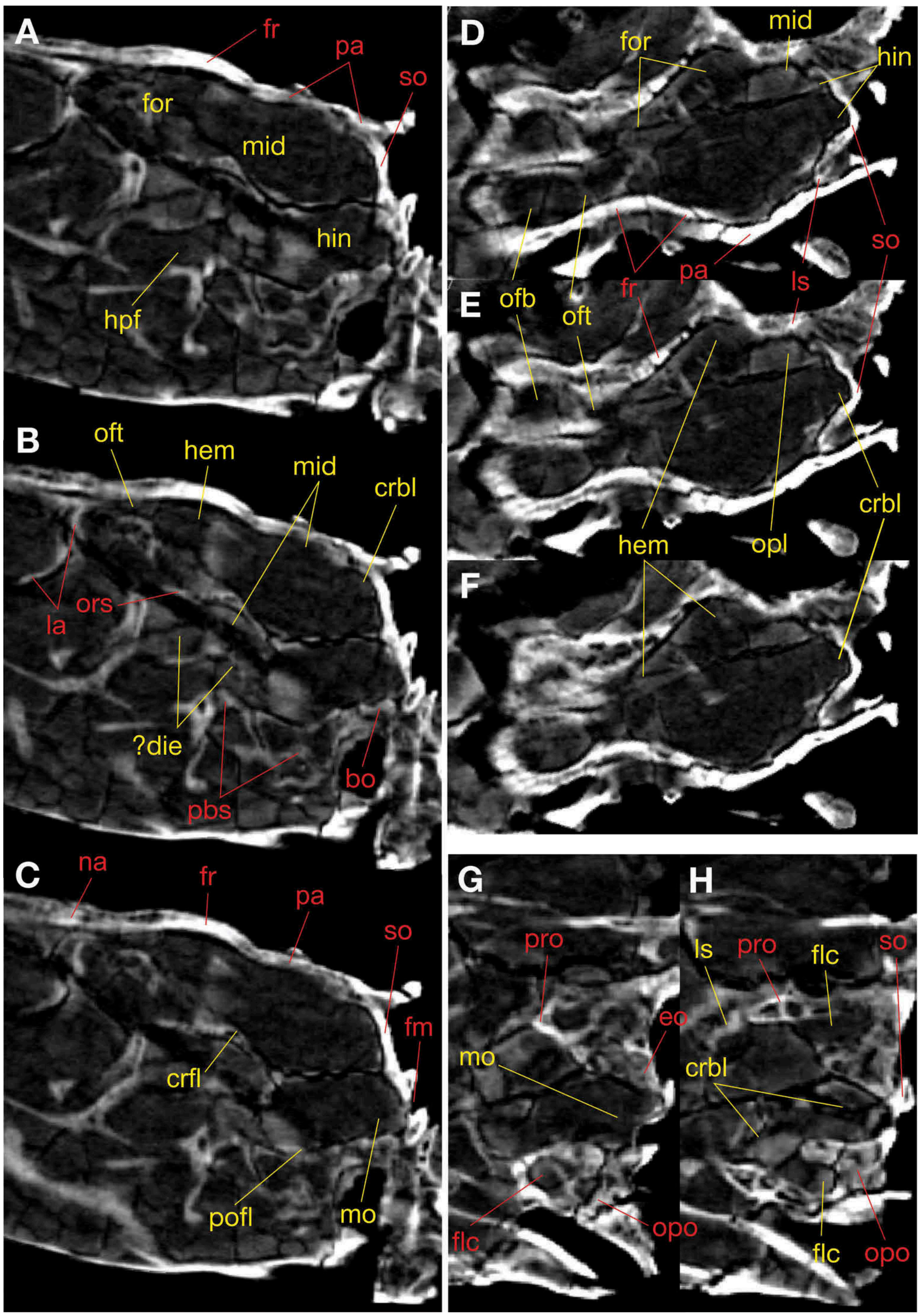

Figure 2. Virtual sections through the neurocranium of *Dilong paradoxus*. A-C, Parasagittal sections through the endoneurocranium. **D-F**, Frontal sections through the endoneurocranium. **G, H.** Frontal sections through the hindbrain. Abbreviations: bo, basioccipital; crbl, cerebellum; crfl, cerebral flexure; eo, exoccipital; flc, flocculus; fm, foramen magnum; fr, frontal; for, forebrain; fr, frontal; hem, cerebral hemispheres; hin, hindbrain; la, lacrimal; ls, laterosphenoid; mid, midbrain; mo, medulla oblongata; na, nasal; ofb, olfactory bulb; oft, olfactory tracts; opl, optic lobe; opo, opisthotic; ors, orbitosphenoid; pa, parietal; pbs, parabasisphenoid; pofl, pontine flexure; pro, prootic; so, supraoccipital.

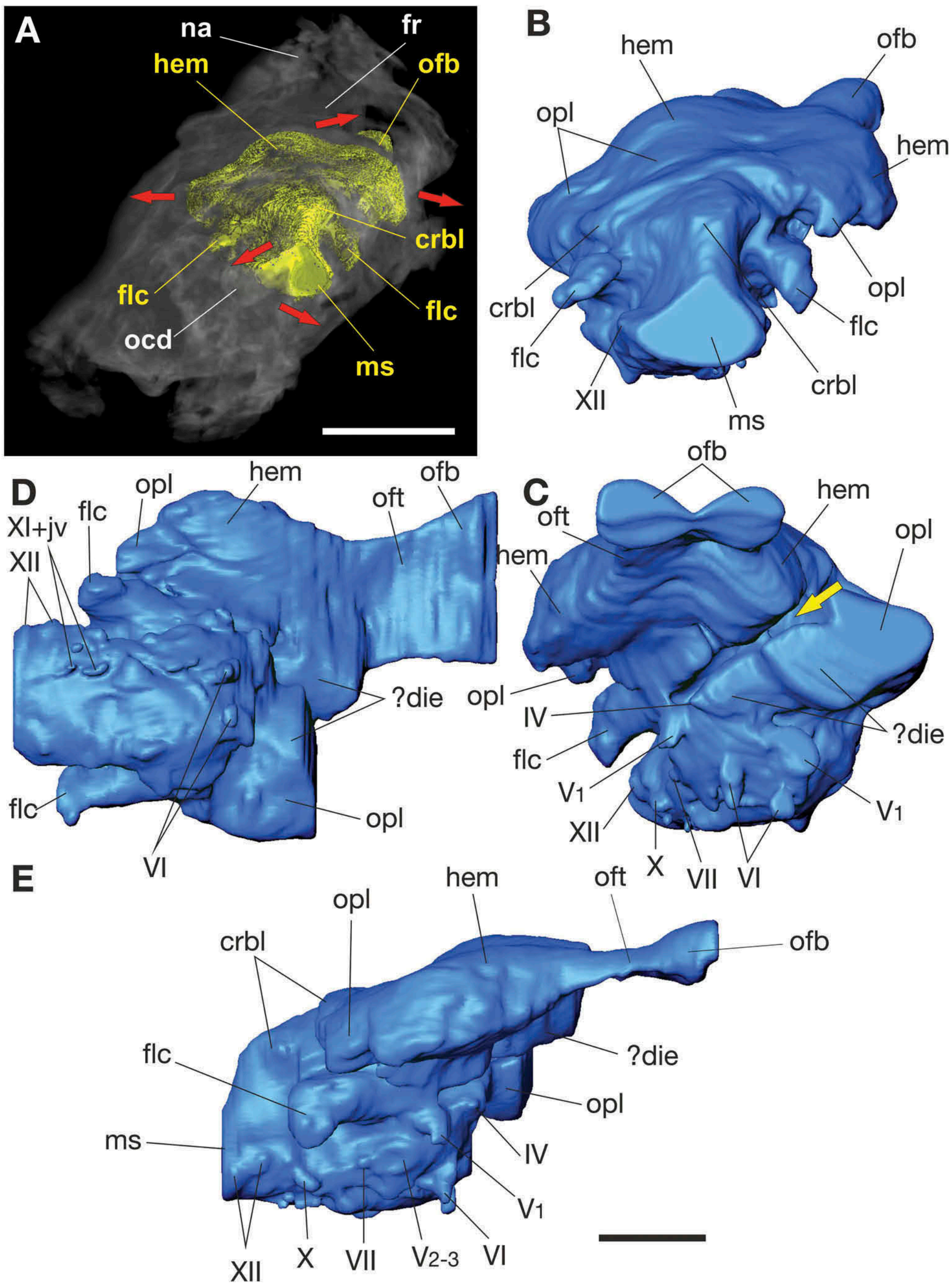

Figure 3. **Endocast of the basal tyrannosauroid *Dilong paradoxus* from the Lower Cretaceous of China. A**, posterior view; Red arrows correspond to directions of major dislocations. **B-E**, The virtual endocast in posterior, anterior, ventral and right lateral views; note yelloe arrow showing the major breakage inside the braincase. Abbreviations: crbl, cerebellum; die, diencephalon; flc, flocculus; hem, cerebral hemispheres; jv, jugular vein; ms, medulla spinalis; ofb, olfactory bulb; oft, olfactory tract; opl, optic lobes; IV, trochlear nerve; V_1, ophthalmic branch of trigeminal nerve; $V_{2–3}$, maxillo-mandibular branch of trigeminal nerve; VI, abducens nerve; VII, facial nerve; IX, glossopharyngeal nerve; X, vagus nerve; XII, hypoglossal nerve. Scale 15 mm (A); 10 mm (B-E).

The proposed size of the region would suggest a rather advanced capability of odor detection in *Dilong*.

The cerebral hemispheres have a pyriform shape. In comparison with *Gorgosaurus* and tyrannosaurines (Brochu 2000, 2003; Saveliev and Alifanov 2007; Witmer and Ridgely 2009; Bever et al. 2011) the cerebrum is far more caudolaterally expanded in *Dilong*, and comprise 2.5 cm^3, ~ 30% of the total reconstructed volume (TRV). This volume implies that the forebrain, the processing centrum of perceptual, vocal and cognitive stimuli, likely was of particular importance to *Dilong*. No imprint of the pineal gland is seen between the hemispheres.

The optic lobes are preserved as distinct swellings placed laterally and somewhat ventrally and are partially overlapped by the hemispheres. The optic lobes likely rotated ventrolaterally as they significantly overlap the rostral hindbrain as in maniraptorans including *Archaeopteryx* (Domínguez Alonso et al. 2004; Kundrát 2007; Witmer and Ridgely 2009). Dorsally, the optic lobes are almost as broad as the cerebral hemispheres.

The cerebellum is considerably enlarged, up to 65% of the maximum width of the brain. It is partly wedged between the optic lobes, and thus approaches the caudal margin of the cerebral hemispheres. *Dilong* has well-marked cerebral and pontine flexures. The pontine flexure (the bend between the midbrain and the hindbrain) is more pronounced and has an angle of about 90°, reminiscent of the condition seen in more advanced maniraptorans (Balanoff et al. 2013). Posteriorly, the cerebellum slopes abruptly prior to the foramen magnum. This same shape is present in *Nanotyrannus* and some maniraptoran theropods (Kundrát 2007; Witmer and Ridgely 2009) including *Archaeopteryx* (Domínguez Alonso et al. 2004) but contrasts with the conditions seen in large-bodied tyrannosaurids (Brochu 2000; Saveliev and Alifanov 2007; Witmer and Ridgely 2009) including *Tyrannosaurus* (Figure 3(c,d)). In the latter, the caudal part of the cerebellar endocast is elongated and slopes gradually prior to the foramen magnum. The cerebellar surface shows no traces of foliar structures. The volume of the metencephalon including the cerebellum, auriculae cerebelli (flocculi), and dural venous sinuses is 3.9 cm^3 (47% of TRV). Compared to tyrannosaurids (Witmer and Ridgely 2009), the flocculi of *Dilong* are enlarged, extending as far caudally as the posterior semicircular canal. In contrast to *Allosaurus* and the tyrannosaurids (Witmer and Ridgely 2009) except *Alioramus* (Bever et al. 2011) the flocculus does not narrow distally as in therizinosaurids (Lautenschlager et al. 2012) and *Conchoraptor* (Kundrát 2007). It is likely that the enormous flocculus functioned efficiently to integrate sensory stimuli about the head rotation during rapid locomotion.

The inner ear is only partially preserved (Figure 4). The crus communis can be seen branching orthogonally into incomplete posterior (upper part) and anterior (ascending part) semicircular canals (SC). The ascending part of the anterior SC expands caudodorsally beyond the plane of the posterior SC. The crus communis broadens dorsally as in *Alioramus* (Bever et al. 2011), and descends in the antero-ventral direction. In contrast to *Tyrannosaurus* it appears to be angled (anterolateroventrally) at the base as in *Struthiomimus* (Witmer and Ridgely 2009). Roots of the trigeminal, facial, vestibulocochlear, vagal and hypoglossal nerves are present. The ganglion Gasseri has an intracranial position as indicated by the separate projections of the ophthalmic (V_1) and maxilla-mandibular (V_{2-3}) branches of the trigeminal nerve. The abducens nerve is comparatively thick, likely correlating with the large orbit, and suggests an efficiently functioning lateral rectus muscle that controls the abduction of the eyeball. The facial nerve outlet is well separated from that of the V_{2-3} and probably the two did were not transmitted through a common canal as in *Tyrannosaurus* (Witmer and Ridgely 2009). Furthermore, the glossopharyngeal and hypoglossal nerves are topographically much closer to each other in *Dilong* than in *Tyrannosaurus*. Finally, all cranial bones surrounding the cranial cavity and osseous labyrinth are highly pneumatized in *Dilong*.

Morphological disparity in the endocasts of dilong and tyrannosaurus

Dilong and *Tyrannosaurus* represent two extremes for Tyrannosauroidea as far as their body sizes and the geological ages are concerned. Their well-preserved fossils allow study of the evolutionary changes in the ENC and hence modification of the tyrannosauroid central nervous system (CNS) which spanned the Cretaceous period (145–66 Ma). We compare the endocast of *Dilong* (Figure 5(a,b)) with that of *Tyrannosaurus* (FMNH PR 2081). Previous reconstructions of the endocast of FMNH PR 2081 were not precise enough for the purpose of this study (Brochu 2000, 2003) and lacked volumetric data (Witmer and Ridgely 2009). We, therefore, have prepared the endocast *de novo* (Figure 5(c,d)) using the original scan data with the recalculated voxel size of 0.497 x 0.497 x 2.0 mm. The new measurements of the endocast are: maximum length: 263 mm, maximum width: 72 mm, volume: 520.7 cm^3, surface area: 531.5 cm^2.

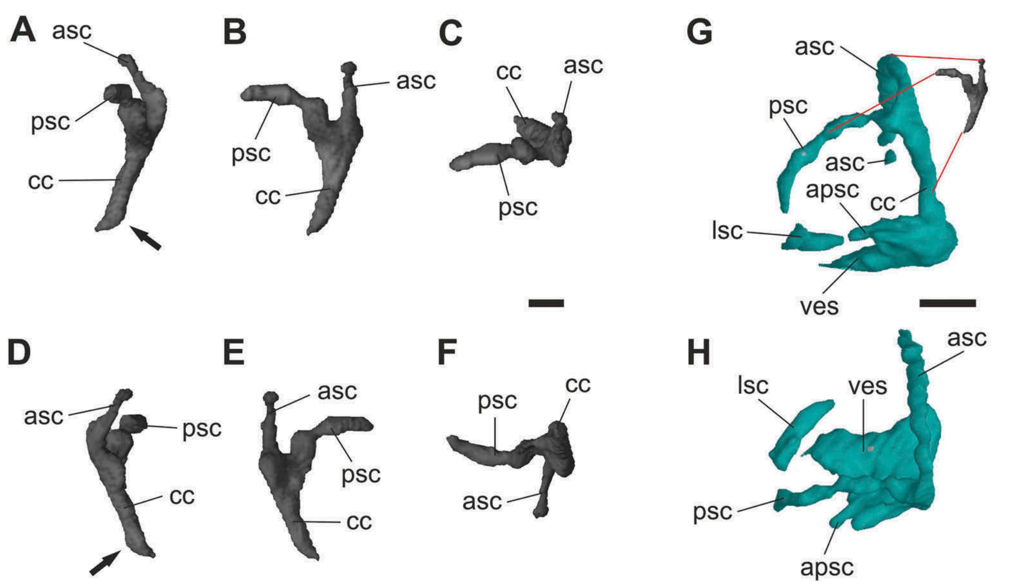

Figure 4. Endocasts of a basally-diverging and a mode derived tyrannosauroid. A, Lateral view of the inner ear endocast of *Dilong*. The arrow points to the ventral angulation of the crus communis. **B**, Posterior view. **C**, Dorsal view. **D**, Medial view. **E**, Anterior view. **F**, Ventral view. **G, H**, Osseous labirynth of *Tyrannosaurus rex* (FMNH PR 2081) in posterior and dorsal view. Note the comparison of the inner ear fragments of *Tyrannosaurus* (blue) and *Dilong* (grey). Abbreviations: apsc, ampula of posterior semicircular canal; asc, anterior semicircular canal; cc, crus communis; lsc, lateral semicircular canal; psc, posterior semicircular canal; ves, vestibule of inner ear. Scale 1.5 mm (A-F); 6.5 mm (G,H).

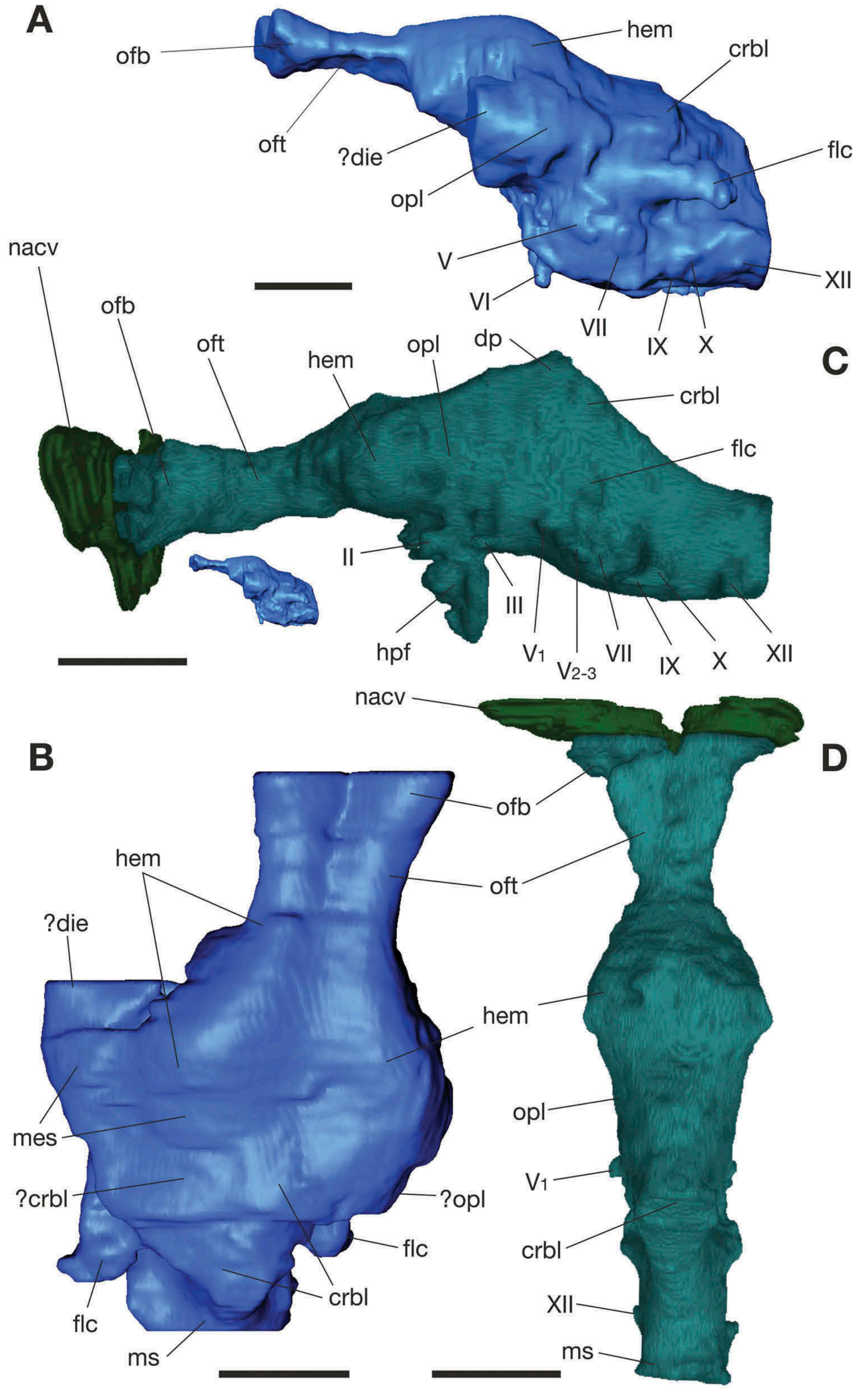

Figure 5. **Endocasts of a basally-diverging and a mode derived tyrannosauroid. A, B,** The virtual endocast of *Dilong paradoxus* in left lateral and dorsal views. **C, D,** The virtual endocast of *Tyrannosaurus rex* (FMNH PR 2081) in left lateral and dorsal views. Note the size of the endocast of *Dilong* adapted to the scale of the *Tyrannosaurus* endocast. Abbreviations: crbl, cerebellum; dp, dorsal peak; flc, flocculus; hem, cerebral hemispheres; hpf, hypophyseal fossa; ms, medulla spinalis; nacv, nasal cavity; ofb, olfactory bulb; oft, olfactory tract; opl, optic lobes; II, optic tract; V, trigeminal nerve; V_1, ophthalmic branch; V_{2-3}, maxillo-mandibular branch; VI, abducens nerve; VII, facial nerve; IX, glossopharyngeal nerve; X, vagus nerve; XII, hypoglossal nerve. Scale 10 mm (A, B); 50 mm (C, D).

These new measurements indicate an endoneurocranial volume for *Tyrannosaurus* that is 62 times larger than that of *Dilong*.

The endocasts of *Dilong* and *Tyrannosaurus* are morphologically disparate. We roughly segmented the endocast of *Dilong* and *Tyrannosaurus* to estimate volumes of the individual regions; e.g. olfactory, prosencephalon, mesencephalon and metencephalon. We quantified differences between regions of these two taxa by calculating their partial/total volume indices (PTV). Our results indicate that during the evolution of tyrannosaurs the olfactory region enlarged (PTV: Tyr-olf: 0.18; Dil-olf: 0.03; this coefficient may be two to three times bigger when including the missing portion of the olfactory bulb (regardless, this does not contradict the conclusion above). The metencephalic region increased relatively proportionally (PTV: Tyr-met: 0.51; Dil-met: 0.47), but the two remaining regions decreased in relative size. The prosencephalon (PTV: Tyr-pro: 0.23; Dil-pro: 0.30) decreased less than mesencephalon (PTV: Tyr-mes: 0.08; Dil-mes: 0.2).

These orientational correlations are congruent with our results of geometric morphometrics of the *Dilong* and *Tyrannosaurus* endocasts expressed on 2D deformation grids (Figure 6). This

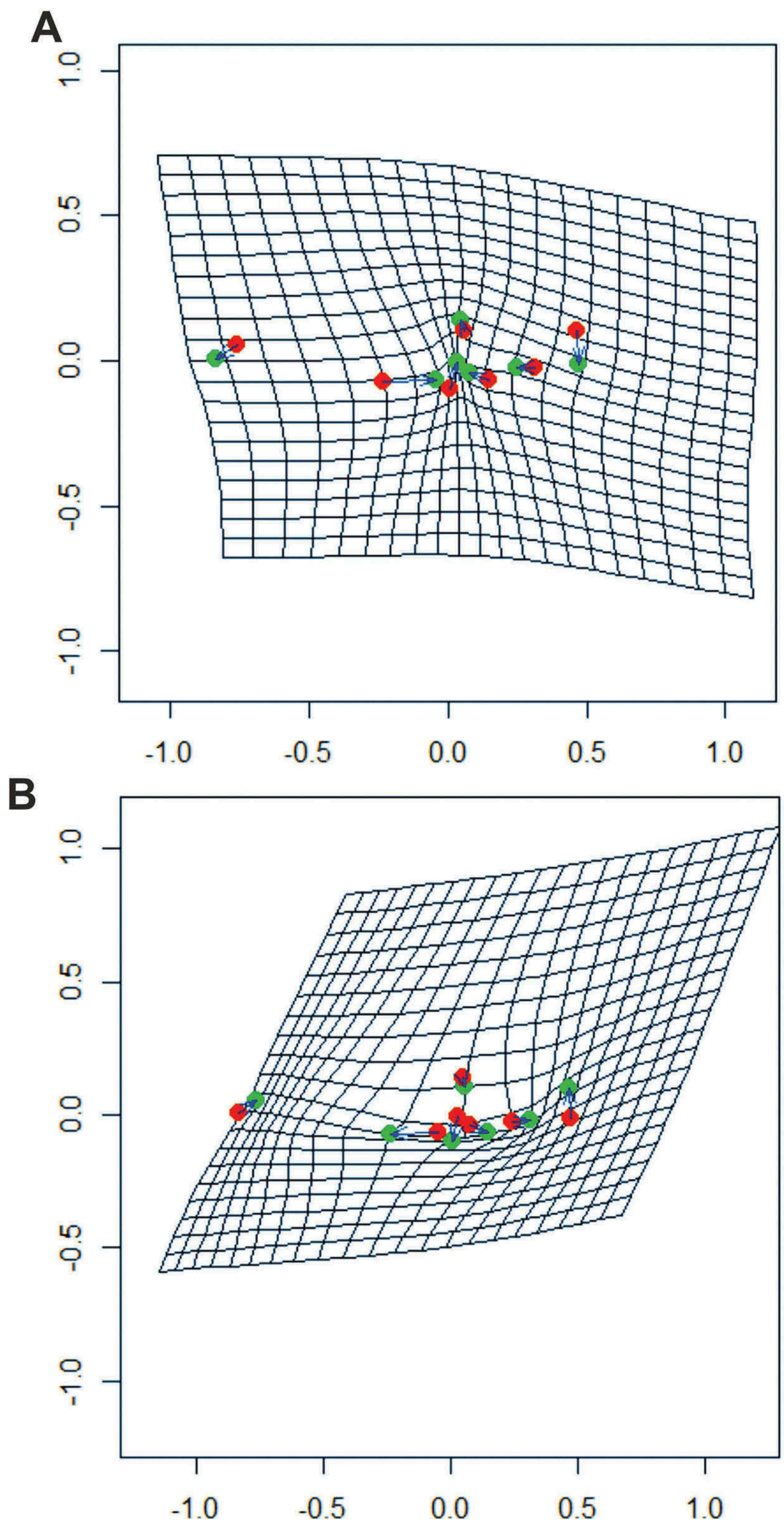

Figure 6. The deformation diagram of changes in landmark positions in 2D. A, Changes in landmark positions from *Dilong* (green dots) to *Tyrannosaurus* (red dots). **B**, Changes in landmark positions from *Tyrannosaurus* (green dots) to *Dilong* (red dots).

analysis was based on anatomically homologous landmarks that were manually positioned either on the outline of or inside the endocast visualized in 2D. The landmarks correspond to comparable positions of the homologous cranial nerves and important angulations of the endocast outlines. The deformation patterns of *Dilong* and *Tyrannosaurus* are derived from a centroid of the two through the procrustes distances. We found that the major shifts in the shape of the endoneurocranium include: 1) general linearization of the tyrannosauroid pattern; 2) rostro-caudal prolongation of the olfactory and posterior metencephalon; 3) abbreviation of the prosencephalon and mesencephalon; and 4) dorsal expansion of the anterior metencephalon.

Variability of the endocast shapes

Nonparametric bootstrap procedure implemented by us confirmed that the biological variability of the shapes is statistically more significant than the error caused by the digitization of the landmarks. Confidence interval (249.6072, 367.0321) based on average partial Prorustes distances of specimens from the sample means, measure of shape variation within samples (Webster and Sheets 2010), does not cover zero. Also boxplot (Figure 7(a)) acknowledged statistically significant difference between partial Procrustes distances in the group of all the observed shapes and in the group of the copies of one individual. Nearest-neighbor analyses by testing the over-dispersion and clustering showed the meaningfulness of the analysis of studied shapes, since they are not just randomly distributed throughout morphospace. Both confidence intervals (−0.3087, −0.1599) and (−0.2563, −0.1005) exclude zero and they suggest that endocast shapes are more tightly clustered than expected under null model. We employ uniform distribution in null hypotheses as we make comparisons among species (Zelditch et al. 2012).

The tangent-space adequacy test (Figure 7(b)) demonstrated that standard statistical moethods such as principal component analysis and regression analysis which require data to be flat Euclidean space can be used (Claude 2008).

Discussion

In the latest Cretaceous, tyrannosauroids were a group of mostly top predators among coelurosaurian theropods, a group of

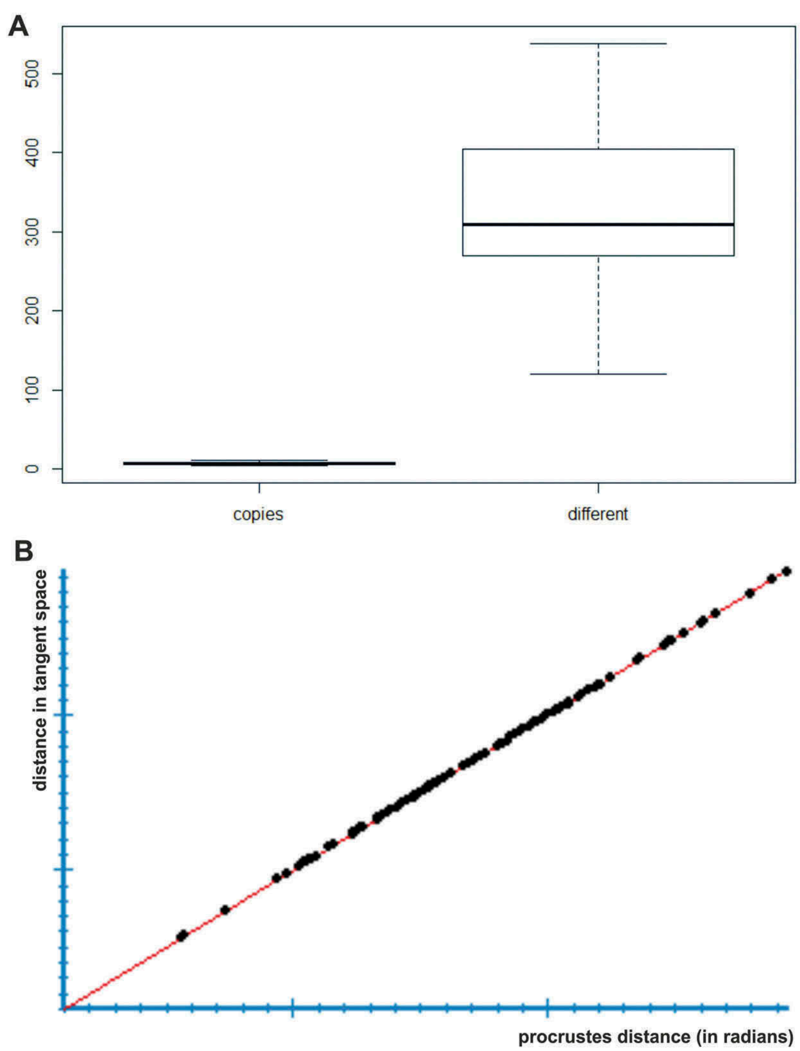

Figure 7. Statistic analysis of the endocast shape variability. A, Boxplot showing partial Procrustes distances in the group of all the observed shapes and in the group of the copies of one individual. **B**, Relationship between the Procrustes distances of the shape space and the Euclidean distances in the tangent shape space (regression with both slope and correlation virtually equal to 1 proved that the approximation is excellent).

derived theropods that includes living birds. Although they have become well known because of their terminal large-bodied forms (e.g. *Tyrannosaurus* – 12 m in length; Holtz 2004), most tyrannosauroids were substantially smaller creatures during the Early Cretaceous (e.g. *Dilong* – 1.6 m; Xu et al. 2004) and Middle to Late Jurassic (e.g. *Guanlong* – 3 m) (Xu et al. 2006). During the middle and Late Cretaceous (Holtz 2004), tyrannosaurids (a more exclusive clade of tyrannosauroids) underwent extensive body size enlargement (gigantism) (Erickson et al. 2004; Brussate et al. 2010a) and became the largest representatives of Coelurosauria. Different tyrannosauroid clades did not evolve gigantism in parallel with each other and this trend likely had different rates in different clades, but it appears body size increase was fastest during the last 10 to 15 million years of tyrannosaur evolution (Carr and Williamson 2004; Holtz 2004; Brusatte et al. 2010a; Brussate et al. 2010b). *Dilong* is the smallest, basally-diverging tyrannosaur known to preserve a complete braincase. This makes it critical in providing insight into the paleoneurology of primitive tyrannosauroids prior to the extensive body enlargement that occurred along the tyrannosauroid lineage.

Recently, a detailed investigation of the endocast of the 6 m long tyrannosaurid *Alioramus* (Brusatte et al. 2009; Bever et al. 2011, 2013) revealed notable differences in configuration of the endocast of this medium-size tyrannosaur and the larger *Tyrannosaurus*. In addition to being long and narrow, the endocast of *Alioramus* also shows several features that are morphologically immediate between *Dilong* and *Tyrannosaurus*. These include: prominent flocular lobe, ventrolaterally displaced distinctive optic lobes, and short broad olfactory tracts. Furthermore *Alioramus* shows that a tyrannosauroid of this size already lacks well-marked pontine flexure, possesses a dorsal peak, and showed moderate expansion of the cerebral hemispheres (Bever et al. 2011). *Alioramus* thus may document plesiomorphic paleoneurological features of tyrannosaurids before the final evolutionary period of their gigantism. *Alioramus*, however, possesses a somewhat enlarged body size (5–6 m; Kurzanov 1976), and therefore likely is not informative about paleoneurological conditions prior to body size enlargement. The paleoneurological data of *Dilong* thus provides an evolutionary stage before significant reconfiguration of the endocast in large-sized tyrannosauroids took place. This reveals a considerably different endoneurocranial pattern at the base of the non-proceratosaurid tyrannosauroid tree. Using *Dilong* as a proxy to infer the plesiomorphic conditions of basal tyrannosauroids reveals that aforementioned features were advanced in numerous aspects compared to those seen in the terminal, giant taxa. Some of these derived characters are visible in *Alioramus* but lost in the endocasts of gigantic tyrannosaurids. Comparisons between *Alioramus* and *Tyrannosaurus* indicate that major linearization and simplification of the endoneurocranium occurred during the evolutionary period of gigantism. This process also includes the relative volumetric decrease of the cerebral and midbrain regions as well as considerable expansion of the interstitial space in the post-cerebral part of the endoneurocranium. These observations indicate that expanded cerebral hemispheres, laterally displaced optic lobes, and enlarged auriculae cerebelli were already present in basal tyrannosauroids and are reminiscent of the conditions present in some derived small-to-medium sized maniraptorans (Hopson 1979; Kundrát 2007; Balanoff et al. 2009, 2013; Witmer and Ridgely 2009).

Furthermore, we plotted the encephalic volumes of *Dilong* and *Tyrannosaurus* and some other theropods against their body mass (Figure 8). This plot shows that although *Dilong* aligned with the range of non-avialan archosaus, it does fall within the upper region zone of this range and close to the maniraptoran theropod *Conchoraptor*. However, based on the 7-landmarks configurations (Figure 9(a,b)), the affinity of *Dilong* with more derived maniraptorans also is only partly supported by principal component analysis (PCA) (Figure 9(c,d)). According to scree plot three principal components should be retained in order to effectively summarized the data since they cover 80% of variance (Rencher and Christensen 2012). Bivariate plots of main three components projections and 3D graph (Figure 10) show that *Dilong* is relatively distant from the tyrannosaurid cluster and occupies a unique position in the PCA morphospace in comparison to all other comparative patterns. The morphospace occupied by *Dilong* is characterized by specific deformation in which the grid is skewed postero-dorsally. The minimum spanning tree

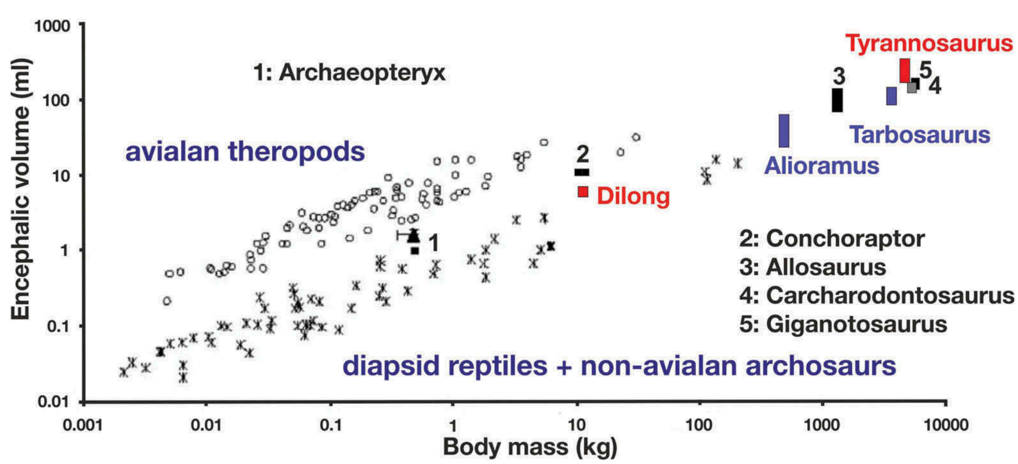

Figure 8. Encephalic volumes plotted against body mass in the avialan and non-avialan diapsids. The plot includes the values of *Archaeopteryx*, the oviraptorid *Conchoraptor, Dilong* (illustrated here for the range of 87–100% of the endocast volume), *Tyrannosaurus* and the other highlighted theropods (illustrated here for the range of 50–100% of the endocast volume).

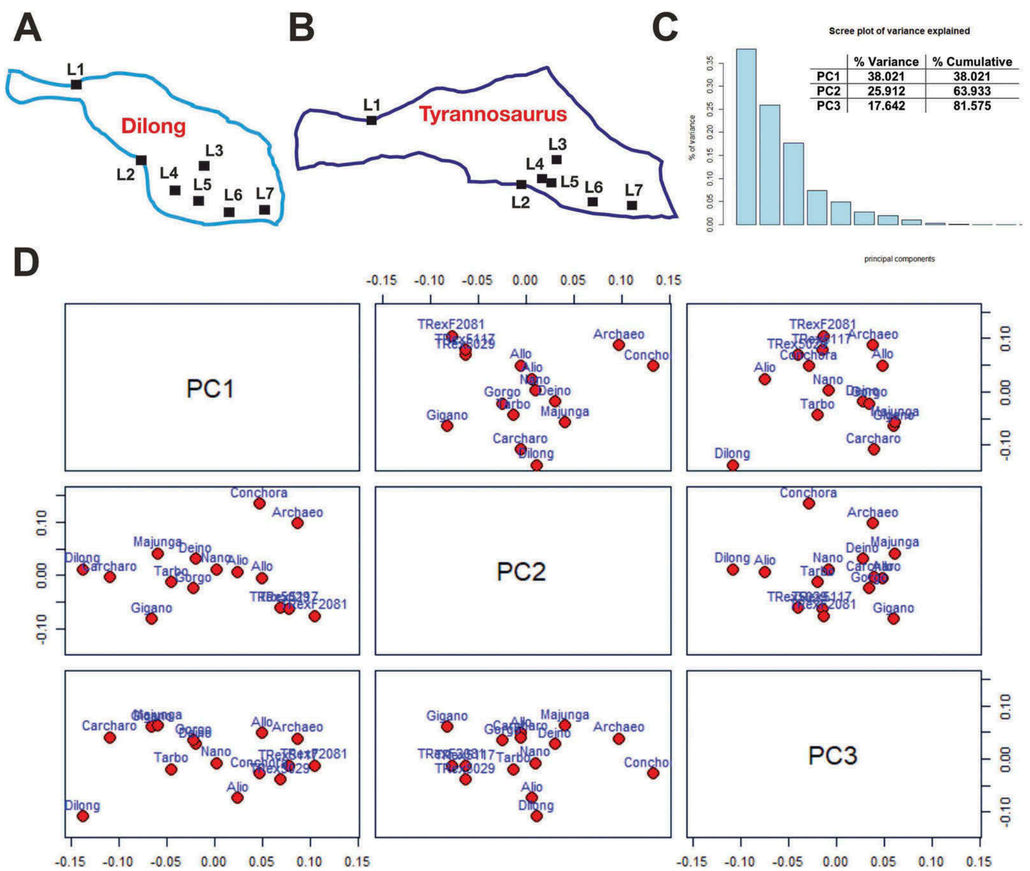

Figure 9. **2D morphometric analysis of the tyrannosauroid endocasts. A, B**, The planar 7-landmark configurations places on the *Dilong* and *Tyrannosaurus* endocast in the left lateral profile image. **C**, Scree plot. **D**,Principal component projections. Landmark definitions: L1: dorsal border between the olfactory tract and the cerebral hemisphere; L2: the cerebral flexure; L3: anterocentral corner of the flocculus; L4: offset of the trigeminal nerve; L5: offset of the facial nerve; L6: offset of the glossopharyngeal nerve; L7: offset of the hypoglossal nerve.

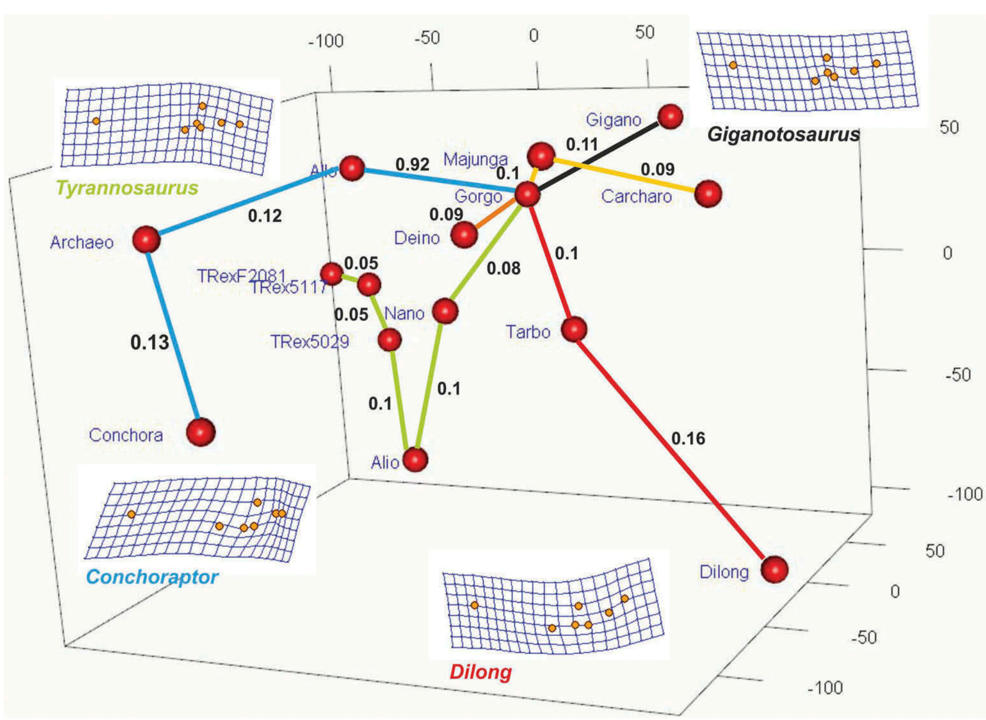

Figure 10. **3D Principal component analysis of the endocast landmarks.** The minimum spanning tree based on minimal mutual distances in morphospace as a measure of shapes similarity: 1. *Alioramus*, 2. *Allosaurus*, 3. *Archaeopteryx*, 4. *Carcharodontosaurus*, 5. *Conchoraptor*, 6. *Deinonychus*, 7. *Dilong*, 8. *Giganotosaurus*, 9. *Gorgosaurus*, 10. *Majungasaurus*, 11. *Nanotyrannus*, 12. *Tarbosaurus*, 13. *Tyrannosaurus* 5029, 14. *Tyrannosaurus* 5117, 15. *Tyrannosaurus* 2081; not the read and green branches that include tyrannosauroid taxa. Grids showing deformations from centroid to extreme values on particular axes.

implies that the *Dilong*′s endoneurocranial shape is most similar to that of *Tarbosaurus*, the Asian version of the Tyrannosaurus rex. Notably, the other gigantic theropods such as *Carcharodontosaurus* and *Giganotosaurus* fall outside of *Tyrannosaurus* cluster, implying that a linear configuration of the endocast evolved convergently in giant theropods. Moreover deformation diagrams of changes in landmark position from centroid revealed the opposite with bending of the deformation grids of *Tyrannosaurus* and *Carcharodontosaurus*, respectively. Finally, plotting the total body length against PC2 variables (Figure 11(a)) provides further evidence that gigantism is highly correlated (strong negative correlation: Pearson′s correlation coefficient = − 0.81, $p < 0.001$; Spearman correlation coefficient: − 0.86, $p < 0.001$; regression line: body length = 7.6233 – 60.9253xPC2) with the endocast morphs. We have also identified the strong correlation when plotting the body weight again PC2 variables (Figure 11(b)). Both somatic parameters might indeed play a critical role in a novel adaptation of the tyrannosaurid ENC that appears phenotypically more primitive than that in the basal most non-proceratosaurid tyrannosauroid, *Dilong*, and converges on the pattern seen in the non-coelurosaurian theropods (Figure 12).

We conclude that the endoneurocranial configuration was far more comparable to advanced morphology in the basally-diverging *Dilong* than it was in the terminal gigantic forms of tyrannosauroid such as *Gorgosaurus* and *Tyrannosaurus* (Hopson 1979; Witmer and Ridgely 2009). We hypothesize that the morphological disparity of the two phylogenetically opposite patterns is coupled with gigantism-related trends that occurred in the evolution of tyrannosauroids. The most obvious modification pertained to a gradual linearization of the endocast that obscures those features that are present in the endocasts of

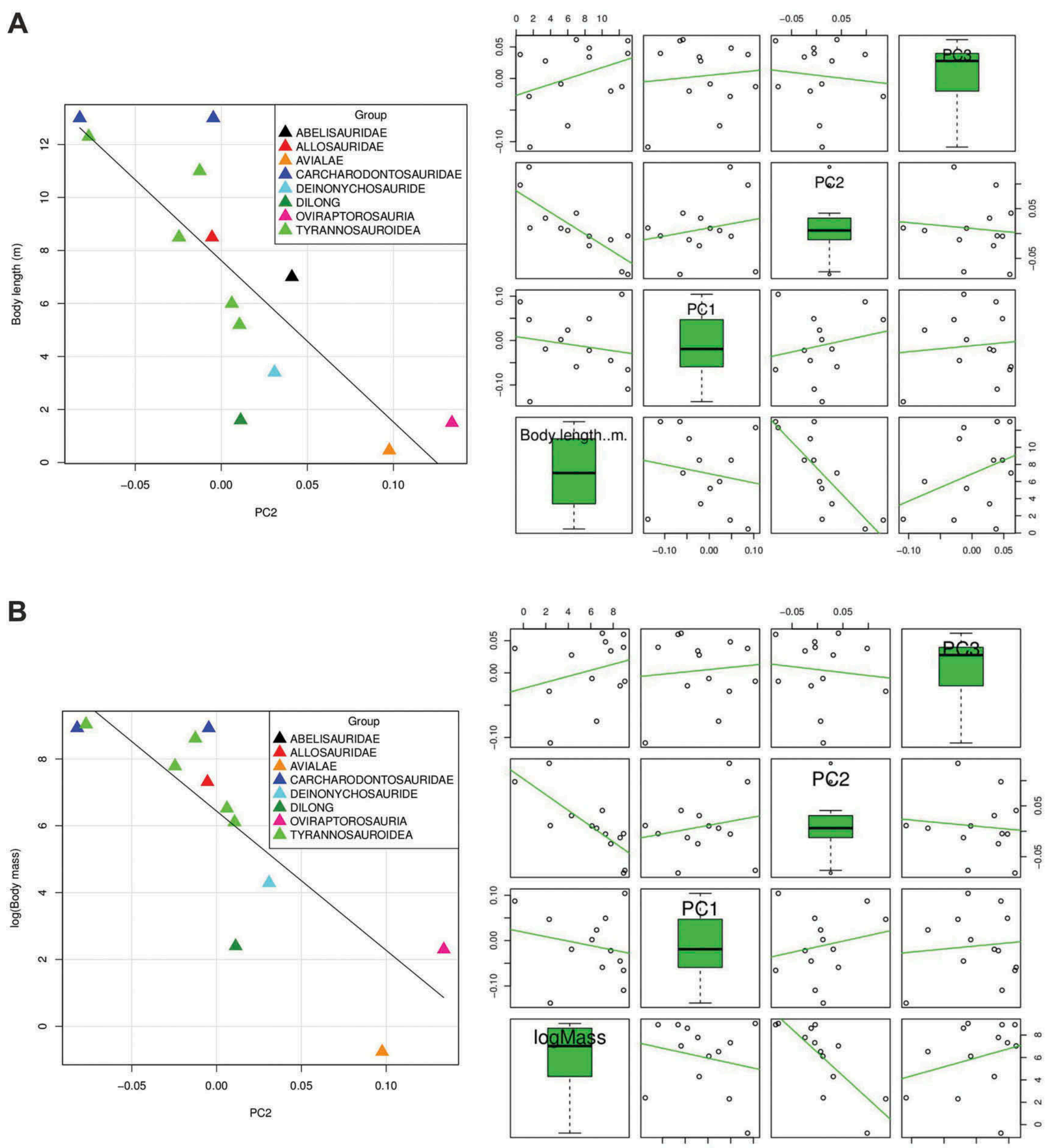

Figure 11. **Strong correlation between body length and PC2.A**, Body length x PC2. **B**, Body weight x PC2.

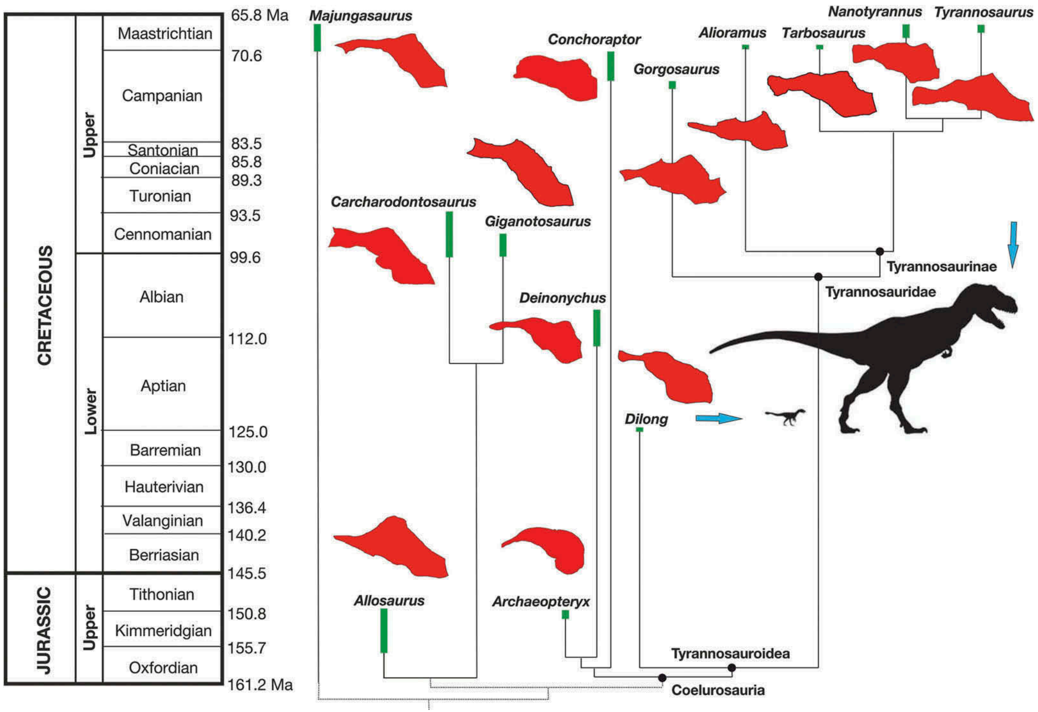

Figure 12. Time-calibrated phylogeny showing the endoneurocranial morphology within Tyrannosauroidea, Maniraptora and other non-coelurosaurian theropods.

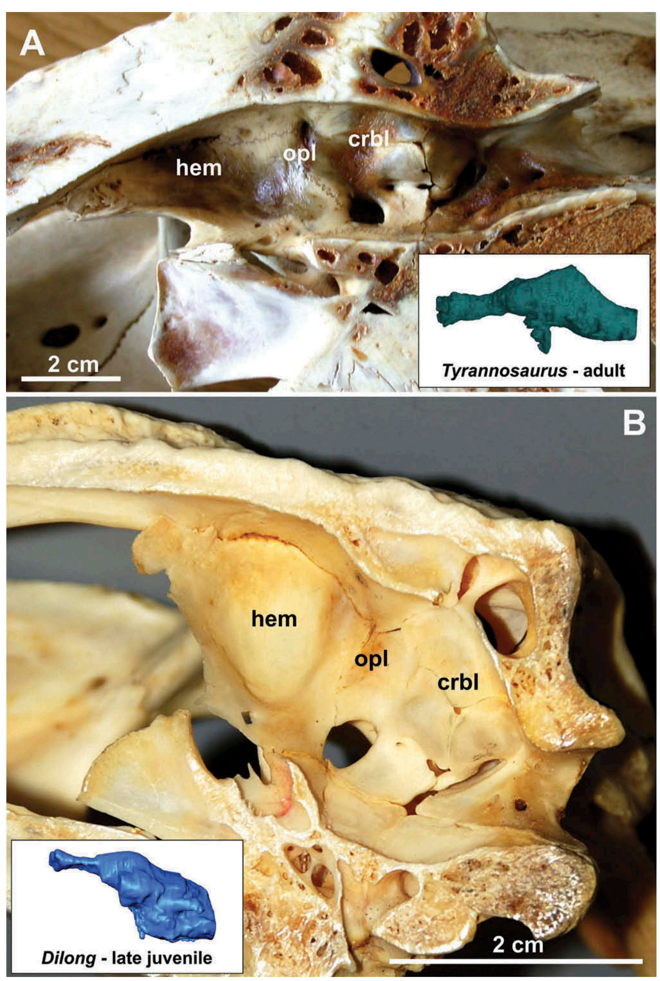

Figure 13. Size-depending configurations of the endoneurocranial cavity in modern crocodilian. A, The linearly shaped, thick-walled endoneurocranium of the fully grown individual of the large size taxon: *Crocodylus porosus*; note similar spatial arrangement in *Tyrannosaurus*. **B**, The superimposed, thin-walled endoneurocranium of the juvenile individual of the middle size taxon: *Alligator mississippiensis*; note morphological similarities with *Dilong*.

Dilong or *Alioramus*. The size-dependent trend in shaping the endoneurocranial cavity, from S-shaped to linear configuration, is also the phenomenon in closest living toothed relatives of dinosaurs, the modern crocodilians (Figure 13). We suggest that the linearly organized brains (as reflected in our endocast study) of gigantic tyrannosaurs likely represent a secondary acquisition, and does not reflect the most advanced conditions of the clade Tyrannosauroidea.

Acknowledgments

We thank P. Makovicky for consulting with us the scan parameters of the *Tyrannosaurus* Sue (FMNH). Amy Balanoff and Stephen Brusatte pre-reviewed an earlier version of drafts and greatly improved the manuscript with their critical comments and suggestions. This work was supported by the grant of Center for Interdisciplinary Biosciences, Technology and Innovation Park, University of Pavol Jozef Šafárik in Košice (Slovakia), the National Natural Science Foundation of China (41120124002 and 41688103), and the Czech Science Foundation (P302/12/1207).

Disclosure statement

No potential conflict of interest was reported by the authors.

Funding

This work was supported by the Grantová Agentura České Republiky [P302/12/1207];National Natural Science Foundation of China [41120124002 and 41688103];Center for Interdisciplinary Biosciences, Technology and Innovation Park, University of Pavol Jozef Šafárik in Košice

Notes on contributor

Martin Kundrát, X.X., and Y.G. designed the project, D.C. performed the CT scanning. M.K. analyzed and interpreted the results, and wrote the paper. M.K. performed the 3D modelling. M.H., A.G. and M.K. conducted geometric morphometrics and biostatistics analysis.

ORCID

Martin Kundrát http://orcid.org/0000-0001-9361-2273

References

Adams DC, Collyer ML, Kaliontzopoulou A 2018. Geomorph: geometric morphometric analyses of 2D/3D landmark data. https://CRAN.R-project.org/package=geomorph.

Alifanov VR, Saveliev SV. 2011. Brain structure and neurobiology of alvarezsaurians (Dinosauria), exemplified by *Ceratonykus oculatus* (Parvicursoridae) from the late cretaceous of Mongolia. Paleontol J. 45:183–190.

Averianov AO, Krasnolutskii SA, Ivantsov SV. 2010. A new basal coelurosaur (Dinosauria: theropoda) from the middle Jurassic of Siberia. Proc Zool Inst. 314:42–57.

Bakker RT, Williams T, Currie PJ. 1988. *Nanotyrannus*, a new genus of pygmy tyrannosaur, from the latest Cretaceous of Montana. Hunteria. 1:1–30.

Balanoff AM, Bever GS, Ikejiri T. 2010. The braincase of *Apatosaurus* (Dinosauria: sauropoda) based on computed tomography of a new specimen with comments on variation and evolution in sauropod neuroanatomy. Am Mus Novit. 3677:1–32.

Balanoff AM, Bever GS, Rowe TB, Norell MA. 2013. Evolutionary origins of the avian brain. Nature. 501:93–96.

Balanoff AM, Xu X, Kobayashi Y, Matsufune Y, Norell MA. 2009. Cranial osteology of the theropod dinosaur *Incisivosaurus gauthieri* (Theropoda: oviraptorosauria). Am Mus Novit. 3651:1–35.

Bever GS, Brusatte S, Carr TD, Xu X, Balanoff AM, Norell MA. 2013. The braincase anatomy of the late cretaceous dinosaur *Alioramus* (Theropoda: tyrannosauroidea). Bull Am Mus Nat Hist. 376:1–72.

Bever GS, Brusatte SL, Balanoff AM, Norell MA. 2011. Variation, variability, and the origin of the avian endocranium: insights from the anatomy of *Alioramus altai* (Theropoda: tyrannosauroidea). PLoS ONE. 6:e23393.

Brochu CA. 2000. A digitally-rendered endocast for *Tyrannosaurus rex*. J Vert Paleontol. 20:1–6.

Brochu CA. 2003. Osteology of *Tyrannosaurus rex*: insights from a nearly complete skeleton and high-resolution computed tomographic analysis of the skull. Mem Soc Vert Paleontol. 7:1–138.

Brusatte SL, Benson RBJ, Xu X. 2010a. The evolution of large-bodied theropod dinosaurs during the Mesozoic in Asia. J Iber Geol. 36:257–296.

Brusatte SL, Carr TD, Erickson GM, Bever GS, Norell MA. 2009. A long-snouted, multihorned tyrannosaurid from the Late Cretaceous of Mongolia. Proc Natl Acad Sci USA. 106:17261–17266.

Brusatte SL, Carr TD, Norell MA. 2012. The osteology of *Alioramus*, a gracile and long-snouted tyrannosaurid (Dinosauria: theropoda) from the Late Cretaceous of Mongolia. Bull Am Mus Nat Hist. 366:1–197.

Brussate SL, Norell MA, Carr TD, Erickson GM, Hutchinson JR, Balanoff AM, Bever GS, Choiniere JN, Makovicky PJ, Xu X. 2010b. Tyrannosaur paleobiology: new research on ancient exemplar organisms. Science. 329:1481–1485.

Butler AB, Hodos W. 2005. Comparative vertebrate neuroanatomy: evolution and adaptation. Hoboken, NJ: John Wiley & Sons, Inc.

Carr TD. 1999. Craniofacial ontogeny in tyrannosauridae (Dinosauria, Coelurosauria). J Vertebr Paleontol. 19:497–520.

Carr TD, Williamson TE. 2004. Diversity of late Maastrichtian Tyrannosauridae (Dinosauria: theropoda) from western North America. Zool J Linn Soc. 142:479–523.

Claude J. 2008. Morphometrics with R. New York: Springer.

Corfield JR, Wild JM, Hauber ME, Parson S, Kubke MF. 2008. Evolution of brain size in the palaeognath lineage, with an emphasis on New Zealand ratites. Brain Behav Evol. 71:87–99.

Currie PJ. 2003. Cranial anatomy of tyrannosaurid dinosaurs from the late Cretaceous of Alberta, Canada. Acta Pal Pol. 48:191–226.

Domínguez Alonso P, Milner AC, Ketcham RA, Cookson MJ, Rowe TB. 2004. The avian nature of the brain and inner ear of *Archaeopteryx*. Nature. 430:666–669.

Dooling RJ, Lohr B, Dent ML. 2000. Hearing in birds and reptiles comparative hearing: birds and reptiles. In: Dooling RJ, Fay RR, Popper AN, editors. Comparative hearing: birds and reptiles. New York: Springer; p. 308–359.

Dryden IL 2017. Shapes: statistical shape analysis. https://CRAN.R-project.org/package=shapes.

Dryden IL, Mardia KV. 2016. Statistical shape analysis: with applications in R. 2 ed. Hoboken (NJ): Wiley.

Erickson GM, Makovicky PJ, Currie PJ, Norell MA, Yerby SA, Brochu CA. 2004. Gigantism and comparative life-history parameters of tyrannosaurid dinosaurs. Nature. 430:772–775.

Evans DC, Ridgely RC, Witmer LM. 2009. Endocranial anatomy of lambeosaurine hadrosaurids (Dinosauria: ornithischia): a sensorineural perspective on cranial crest function. Anat Rec. 292:1315–1337.

Foote M. 1990. Nearest-neighbor analysis of trilobite morphospace. Syst Zool. 39:371–382.

Fowler DW, Woodward HN, Freedman EA, Larson PL, Horner JR. 2011. Reanalysis of "*Raptorex kriegsteini*": a juvenile tyrannosaurid dinosaur from Mongolia. PLoS ONE. 6:e21376.

Franzosa JW, Rowe T. 2005. Cranial endocast of the Cretaceous theropod dinosaur *Acrocanthosaurus atokensis*. J Vert Paleontol. 25:859–864.

Holtz TR Jr. 2004. Tyrannosauroidea. In: Weishampel DB, Dodson P, Osmólska H, editors. The Dinosauria. Berkeley: Univ. California Press; p. 111–136.

Hopson JA. 1979. Paleoneurology. In: Gans C, editor. Biology of the Reptilia. New York: Academic Press; p. 39–143.

Hullar TE. 2006. Semicircular canal geometry, afferent sensitivity, and animal behavior. Anat Rec. 288A:466–472.
Hurlburt GR, Ridgely RC, Witmer LM. 2013. Relative size of brain and cerebrum in Tyrannosaurus rex: an analysis using brain-endocast quantitative relationships in extant alligators. In: Parris JM, Henderson M, Currie PJ, Koppelhus E, editors. Origin, Systematics, and Paleobiology of the Tyrannosauridae. Bloomington: Indian Univ. Press; p. 135–154.
Hurum JH, Sabath K. 2003. Giant theropod dinosaurs from Asia and North America: skulls of *Tarbosaurus bataar* and *Tyrannosaurus rex* compared. Acta Pal Pol. 48:161–190.
Iwaniuk AN, Lefebvre L, Wylie DRW. 2009. The comparative approach and brain-behaviour relationships: A tool for understanding tool use. Can J Exp Psychol. 63:150–159.
Knoll F, Schwarz-Wings D. 2009. Palaeoneuroanatomy of *Brachiosaurus*. Ann Paléntol. 95:165–175.
Knoll F, Witmer LM, Ortega F, Ridgely RC, Schwarz-Wings D. 2012. The braincase of the basal sauropod dinosaur *Spinophorosaurus* and 3D reconstructions of the cranial endocast and inner ear. PLoS ONE. 7:e30060.
Kundrát M. 2007. Avian-like attributes of a virtual brain model of the oviraptorid *Conchoraptor gracilis*. Naturwiss. 94:499–504.
Kurzanov SM. 1976. A new carnosaur from the late Cretaceous of Nogon-Tsav, Monglia. The Joint Soviet-Mongolian Pal Exped Trans. 3:93–104.
Larsson HCE. 2001. Endocranial anatomy of *Carcharodontosaurus saharicus* (Theropoda: allosauroidea) and its implications for theropod brain evolution. In: Tanke DH, Carpenter K, editors. Mesozoic Vertebrate Life. Bloomington: Indiana University Press; p. 19–33.
Larsson HCE, Sereno PC, Wilson JA. 2000. Forebrain enlargement among nonavian theropod dinosaurs. J Vertebr Paleontol. 20:615–618.
Lautenschlager S, Hübner T. 2013. Ontogenetic trajectories in the ornithischian endocranium. J Evol Biol. 26:2044–2050.
Lautenschlager S, Rayfield EJ, Altangerel P, Zanno LE, Witmer LM. 2012. The endocranial anatomy of Therizinosauria and its implications for sensory and cognitive function. PLoS ONE. 7:e52289.
Lauters P, Vercauteren M, Bolotsky YL, Godefroit P. 2013. Cranial endocast of the lambeosaurine hadrosaurid *Amurosaurus riabinini* from the Amur region, Russia. PLoS ONE. 8:e78899.
Loewen MA, Irmis RB, Sertich JJW, Currie PJ, Sampson SD. 2013. Tyrant dinosaur evolution tracks the rise and fall of Late Cretaceous oceans. PLoS ONE. 8:e79420.
Lü J, Yi L, Brusatte SL, Yang L, Li H, Chen L. 2014. A new clade of Asian Late Cretaceous long-snouted tyrannosaurids. Nat Commun. 5:3788.
Mades JH. 1974. A new theropod dinosaur from the Upper Jurassic of Utah. J Paleontol. 48:27–31.
Osborn HF. 1912. Crania of *Tyrannosaurus* and *Allosaurus*. Mem Am Mus Nat Hist. 1:1–30.
Osmólska H. 2004. Evidence on relation of brain to endocranial cavity in oviraptorid dinosaurs. Acta Palaeontol Pol. 49:321–324.
Pan Y, Sha J, Zhou Z, Fürsich FT. 2013. The Jehol Biota: definition and distribution of exceptionally preserved relicts of a continental Early Cretaceous ecosystem. Cret Res. 44:30–38.
Paradis E, Claude J, Strimmer K. 2004. APE: analyses of phylogenetics and evolution in R language. Bioinformatics. 20:289–290.
Paulina-Carabajal A. 2012. Neuroanatomy of titanosaurid dinosaurs from the Upper Cretaceous of Patagonia, with comments on endocranial variability within Sauropoda. Anat Rec. 295:2141–2156.
Paulina-Carabajal A, Canale JI. 2010. Cranial endocast of the carcharodontid theropod *Giganotosaurus carolinii* Coria & Salgado, 1995. N Jb Geol Paläont Abh. 258:249–256.
Paulina-Carabajal A, Currie PJ. 2012. New information on the braincase of *Sinraptor dongi* (Theropoda: allosauroidea): ethmoidal region, endocranial anatomy, and pneumaticity. Vert PalAs. 4:85–101.
Paulina-Carabajal A, Succar C. 2015. The endocranial morphology and inner ear of the abelisaurid theropod *Aucasaurus garridoi*. Acta Palaeontol Pol. 60(1):141–144.
R Core Team. 2018. R: A Language and Environment for Statistical Computing. Vienna (Austria): R Foundation for Statistical Computing. http://www.R-project.org/
Rauhut OWM, Milner AC, Moore-Fay S. 2010. Cranial osteology and phylogenetic position of the theropod dinosaur *Proceratosaurus bradleyi* (Woodward, 1910) from the Middle Jurassic of England. Zool J Linn Soc. 158:155–195.
Rencher AC, Christensen WF. 2012. Methods of Multivariate Analysis. 3rd ed. New Jersey: John Wiley & Sons.
Rich TH, Rich PV. 1988. A juvenile dinosaur brain from Australia. Natl Geogr Res. 4:148.
Rogers SW. 1998. Exploring dinosaur neuropaleobiology: computed scanning and analysis of an *Allosaurus fragilis* endocast. Neuron. 21:673–679.
Rohlf FJ 2010. *Tps Series*. Department of Ecology and Evolution, State University of New York, Stony Brook (New York). Available: http://life.bio.sunysb.edu/morph/. Accessed 2018 June 26.
Sampson SD, Witmer LM. 2007. Craniofacial Anatomy of *Majungasaurus crenatissimus* (Theropoda: abelisauridae) from the Late Cretaceous of Madagascar. J Vert Paleontol. 27:32–104.
Sanders RK, Smith DK. 2005. The endocranium of the theropod dinosaur *Ceratosaurus* studied with computed tomography. Acta Palaeontol Pol. 50:601–616.
Saveliev SV, Alifanov VR. 2007. A new study of the brain of the predatory dinosaur *Tarbosaurus bataar* (Theropoda, Tyrannosauridae). Paleont J. 41:281–289.
Sereno PC, Tan L, Brusatte SL, Kriegstein HJ, Zhao X, Cloward K. 2009. Tyrannosaurid skeletal design first evolved at small body size. Science. 326:418–422.
Sereno PC, Wilson JA, Witmer LM, Whitlock JA, Maga A, Ide O, Rowe TA. 2007. Structural extremes in a Cretaceous dinosaur. PLoS ONE. 2:e1230.
Sol D, Garcia N, Iwaniuk A, Davis K, Meade A, Boyle A, Székely T. 2010. Evolutionary divergence in brain size between migratory and resident birds. PLoS ONE. 5:e9613.
Tsuihiji T, Watabe M, Tsogtbaatar K, Tsubamoto T, Barsbold R, Suzuki S, Lee AH, Ridgely RC, Kawahara Y, Witmer LM. 2011. Cranial osteology of a juvenile specimen of *Tarbosaurus bataar* (Theropoda, Tyrannosauridae) from the Nemegt Formation (Upper Cretaceous) of Bugin Tsav, Mongolia. J Vertebr Paleontol. 31:497–517.
Webster M, Sheets HD. 2010. A practical introduction to landmark-based geometric morphometrics. Quant Meth Paleobiol. 16:163–188.
Witmer LM, Ridgely RC. 2008. Structure of the brain cavity and inner ear of the centrosaurine ceratopsid *Pachyrhinosaurus* based on CT scanning and 3D visualization. In: Currie PJ, Langston W, Tanke DH, editors. A new horned Dinosaur from an Upper Cretaceous bone bed in Alberta. Ottawa: NRC Research Press; p. 117–144.
Witmer LM, Ridgely RC. 2009. New insights into the brain, braincase, and ear region of tyrannosaurs (Dinosauria: theropoda), with implications for sensory organization and behavior. Anat Rec. 292:1266–1296.
Witmer LM, Ridgely RC. 2010. The Cleveland tyrannosaur skull (*Nanotyrannus* or *Tyrannosaurus*): new findings based on CT scanning, with special reference to the braincase. Kirtlandia. 57:61–81.
Witmer LM, Ridgely RC, Dufeau DL, Semones MC. 2008. Using CT to peer into the past: 3D visualization of the brain and ear regions of avialans, crocodilians, and nonavian dinosaurs. In: Endo H, Frey R, editors. Anatomical Imaging: towards a New Morphology. Tokyo: Springer-Verlag, 2008; p. 67–87.
Xu X, Clark JM, Forster CA, Norell MA, Erickson M, Eberth DA, Jia C, Zhao Q. 2006. A basal tyrannosauroid dinosaur from the Late Jurassic of China. Nature. 439:715–718.
Xu X, Norell MA, Kuang X, Wang X, Zho Q, Jia C. 2004. Basal tyrannosauroids from China and evidence for protofeathers in tyrannosauroids. Nature. 431:680–684.
Zelditch ML, Swiderski DL, Sheets HD. 2012. Geometric morphometrics for Biologists. 2 ed. Amsterdam: Academic Press.
Zelenitsky DK, Therrien F, Ridgely RC, McGee AR, Witmer LM. 2011. Evolution of olfaction in non-avian theropod dinosaurs and birds. Proc R Soc B. 278:3625–3634.
Zhou C-F, Gao K-Q, Fox R, Du X-K. 2007. Endocranial morphology of psittacosaurs (Dinosauria: ceratopsia) based on CT scans of new fossils from the Lower Cretaceous, China. Palaeoworld. 16:285–293.